DISTANCE MEASURES IN GRAVITATIONAL-WAVE ASTROPHYSICS AND COSMOLOGY

Hsin-Yu Chen[1], Daniel E. Holz[1], John Miller[2], Matthew Evans[2], Salvatore Vitale[2], Jolien Creighton[3]
Draft version September 26, 2017

ABSTRACT

We present quantities which characterize the sensitivity of gravitational-wave observatories to sources at cosmological distances. In particular, we introduce and generalize the horizon, range, response, and reach distances. These quantities incorporate a number of important effects, including cosmologically well-defined distances and volumes, cosmological redshift, cosmological time dilation, and rate density evolution. In addition, these quantities incorporate unique aspects of gravitational wave detectors, such as the variable sky sensitivity of the detectors and the scaling of the sensitivity with inverse distance. An online calculator (`http://gwc.rcc.uchicago.edu`) and python notebook (`https://github.com/hsinyuc/distancetool`) to determine GW distances are available. We provide answers to the question: "How far can gravitational-wave detectors hear?"

1. INTRODUCTION

LIGO has officially ushered in the era of gravitational-wave (GW) astrophysics. The first detections have included binary black hole systems well into the Hubble flow where cosmological effects start to become important; for example, the redshift of GW170104 is $z \sim 0.2$ (Abbott et al. 2017b). As GW detectors improve, and as the network of GW detectors is expanded (Hild et al. 2011; Sathyaprakash et al. 2012; Abbott et al. 2016b,a), we expect to detect binaries to ever greater distances. With this in mind, in what follows we present a number of quantities to summarize the sensitivity of detectors taking into account cosmological effects such as time dilation and cosmological volume.

Furthermore, there are some characteristics of GW astronomy that are fundamentally different from "traditional" electromagnetic (EM) astronomy, and this means that quantities used to summarize EM telescopes need to be adjusted for GW telescopes [4]. Quantities such as magnitude limit, sky brightness, B-band luminosity, and Vega magnitudes need to be replaced.

One particularly important distinction between optical and GW telescopes is their differing sky response. GW telescopes are sensitive to sources on the entire sky, although the sensitivity varies greatly depending on the particular sky location. The average distance to which a GW telescope can detect a given source varies greatly depending on where the source is on the sky *relative to the detector* (i.e., as measured in the detector [i.e., Earth!] frame, not a fixed location on the sky). The quantities we propose below take this antenna pattern sensitivity into account.

2. DISTANCE MEASURES

The sensitivity of a GW detector is a function of two factors: the properties of the detector and the properties of the source of interest. For any fixed detector noise curve (e.g., LIGO O3) and any fixed binary coalescence system (e.g., 30–30 $M_\odot$ binary black holes), we are interested in summarizing the sensitivity of that detector to that given source. In particular, some quantities of interest include:

- **Horizon distance, d^{h}:** The farthest luminosity distance the given source could ever be detected above threshold (i.e., at optimal sky location and binary inclination/orientation). Throughout this paper we assume the detection threshold is approximated by a matched-filter signal-to-noise ratio (SNR), ρ_{th}, of 8 (Thorne 1987; Allen et al. 2012). See below for more detail.

- **Redshifted Volume, V_z:** The spacetime volume surveyed per unit detector time, in units of Mpc^3. This is the comoving volume (see, e.g., Hogg (1999)), with the addition of a $(1 + z)$ factor to account for time dilation. If you multiply V_z by the constant comoving source-frame rate density, you get the detection rate. This quantity is sky-averaged and inclination/orientation averaged. In detail:

$$V_z =$$

$$\frac{\int_{D_c < d^{\mathrm{h}}} \frac{D_c^2}{1+z(D_c)} dD_c \, d\Omega \, \sin \iota \, d\iota \, d\psi}{\int \sin \iota \, d\iota \, d\psi}, \quad (1)$$

where D_c is the comoving distance and Ω is the solid angle on the sky. $d^{\mathrm{h}}(\theta, \phi, \psi, \iota)$ is the comoving distance for which SNR $= \rho_{\mathrm{th}}$ for a binary with inclination ι [5], orientation ψ, and along the sky direction (θ, ϕ).

- **Range distance, R:** The distance for which $4/3\pi R^3 = V_z$, where V_z is defined above. This is the radius of a Euclidean sphere which would contain the same volume as the true redshifted volume. At low redshift ($z \lesssim 1$) this quantity is well

[1] University of Chicago, Chicago, Illinois 60637, USA
[2] LIGO, Massachusetts Institute of Technology, Cambridge, Massachusetts 02139, USA
[3] University of Wisconsin-Milwaukee, Milwaukee, Wisconsin 53201, USA

[4] In many ways GW astronomy is closer to radio astronomy, where the signals are coherent and beam patterns must be incorporated. See the discussion below.

[5] The inclination is the angle between the binary rotational axis and the line-of-sight direction.

approximated by the horizon distance divided by 2.264 (Finn & Chernoff 1993) and has historically been called the "sensemon distance"; see Sec. 4.3 for more detail.

- **Response distance, d_x^{p}**: The luminosity distance *at* which $x\%$ of the sources would be detected, for sources placed isotropically on the sky with random inclinations/orientations, *but with all sources placed at exactly this distance*. Note that d_0^{p} corresponds to the horizon distance. A binary at distance d_x^{p} would have a maximum possible SNR of ρ, and that ρ would satisfy: $P(\rho_{\mathrm{th}}/\rho) = x$, where P is the cumulative antenna pattern function (see Sec. 4.2).

- **Reach distance, d_x^{r}**: The luminosity distance *within* which $x\%$ of the total detections would take place. d_{50}^{r} corresponds to the median distance of the detected population of sources, and d_{100}^{p} corresponds to the horizon distance. The redshifted volume out to d_x^{r}, divided by the total redshifted volume, V_z, is given by $x\%$. In more detail, we calculate the redshifted volume using Eq. 1, but with the limits of the integration given by $\min(d_x^{\mathrm{r}}, d^{\mathrm{h}})$ instead of d^{h} (where d_x^{r} here is in comoving distance). If we divide this by the total redshifted volume (Eq. 1 with d^{h} in the limit), we find a ratio of $x\%$.

- **SFR Reach distance, d_x^{SFR}**: The same as d_x^{r}, but we now scale the source frame rate density by the star formation rate. This is a very rough approximation to the effect of rate evolution on the detected sample. This is equivalent to the expression for d_x^{r}, but with the volume integrals in V_z weighted by an additional factor of the star formation rate.

- **Average distance, $\bar{d}$**: The average luminosity distance of the detected sample. This is to be compared with the median luminosity distance of the detected sample, given by d_{50}^{r}. This is the same as the volume integrals weighted by the luminosity distance and divide by the total redshifted volume.

- **SFR Average distance, $\bar{d}^{\mathrm{SFR}}$**: The same as the Average distance, but we now additionally scale the source-frame rate density by the star formation rate. This is equivalent to the expression for $\bar{d}$ with an additional factor of the star formation rate in the volume integral in both the numerator and the denominator.

An online calculator to determine these distance measures for a range of sources and detector noise curves is available at http://gwc.rcc.uchicago.edu. Python notebooks are also provided at https://github.com/hsinyuc/distancetool, which provide additional details for how to calculate these expressions.

There are a number of important aspects to these distance quantities:

1. We assume a source is "detected" if the SNR of the source in a single detector with the given noise curve is $\rho > 8$. This threshold is arbitrary, and corresponds roughly to an SNR=12 network threshold for two equivalent detectors; it can be trivially generalized to different thresholds and networks of detectors.

2. All of the quantities above include the effects of redshift on the gravitational waveform (see §4.4, Krolak & Schutz (1987); Holz & Hughes (2005)). The masses quoted are in the *source frame*; the waveform of a 5–5 $M_\odot$ binary at $z = 1$ is identical to the waveform of a 10–10 $M_\odot$ system at $z = 0$, modulo an overall amplitude scaling.

3. All of the Reach quantities need to make assumptions for the source-frame rate density, which is expected to evolve at high redshift. We consider two possibilities: a *constant rate* which assumes that the source population is not evolving in time, and a *SFR rate* which approximates the rate evolution by the star formation rate. Since many population synthesis models suggest that the merger rate will roughly follow the star formation rate (e.g. Dominik et al. 2015), we consider a scenario where the merger rate directly tracks the shape of the cosmic star formation rate, as represented by Eq. 15 of Madau & Dickinson (2014).

4. All of the Reach quantities incorporate *time dilation* by including a $1/(1+z)$ redshift factor to convert the fixed source-frame rate to a detected rate.

5. The Redshifted volume quantity assumes that the sources have a constant source-frame rate density and includes the effect of time dilation and redshift of the waveform.

6. For every distance defined above there is an equivalent redshift, defined straightforwardly from the luminosity distance-redshift relation Hogg (1999).

7. Note that for the sake of definiteness we have assumed the cosmological parameters determined by Planck (Planck Collaboration et al. 2016): $\Omega_m = 0.3065$, $\Omega_\lambda = 0.6935$, $\Omega_k = 0$, $h = 0.679$. Percent level changes in these quantities lead to percent level changes in the distances being quoted.

These aspects are discussed in significantly more detail in Sec. 4.

In Tables 1 and 2 and Figures 1 and 2 we present values for these quantities, for three different classes of compact binary coalescence sources: 1.4–1.4 $M_\odot$, 10–10 $M_\odot$, and 30–30 $M_\odot$ (all masses are in the source frame), and for four different detector sensitivities: O2, O3, 2G [Advanced LIGO design (LIGO Scientific Collaboration et al. 2015)], and 3G. The O2, O3, and 2G curves correspond to the Advanced LIGO second, third, and fifth sensitivity curves in Figure 1 of Abbott et al. (2016b). 3G corresponds to the "Cosmic Explorer (fig 1)" curve of Abbott et al. (2017a). We choose Advanced LIGO and Cosmic Explorer as the representative sensitivities for the second (2G) and the third (3G) generation detectors. There are also other detectors proposing to operate at comparable sensitivities, such as Advanced Virgo (2G, Acernese et al. 2015), KAGRA (2G, Aso et al. 2013), and Einstein Telescope (3G, Hild et al. 2011; Sathyaprakash et al. 2012; Abbott et al. 2016a).

For the inspiral-merger-ringdown waveforms, for 1.4–1.4 $M_\odot$ binaries we use the TaylorF2 waveform (Sathyaprakash & Dhurandhar 1991) [6] , and for the 10–10 $M_\odot$ and 30–30 $M_\odot$ binaries we use the IMR-PhenomD waveform (Khan et al. 2016) [7] . We assume aligned spin and ignore precession.

3. COMPARISON OF DISTANCE MEASURES

The different distance quantities enumerated in the previous section represent different ways to encapsulate the performance of a detector to a given source.

The Horizon Distance gives a clear representation of the farthest possible detection. However, because the detector response patterns are not spherical, this quantity is not representative of the general population. Unlike in the EM case, where a large fraction of sources lie near the maximum distance, in the GW case most sources lie significantly closer than the Horizon.

The Redshifted Volume is useful because it gives immediate intuition for how the detection rate scales with sensitivity. If this quantity doubles, then the expected detection rate doubles as well (assuming a constant source-frame rate density).

The Response is useful if one is interested in characterizing a GW detector independent of any assumptions about the intrinsic rates of the source. This quantity summarizes the impact of the antenna pattern and the overall sensitivity of the detector. (see Sec. 4.2).

If one is interested in the median or average distance to which a population of binaries might be detected, then the Reach distances are more appropriate. These numbers depend on assumptions for the source-frame rate density. The "default" assumption is that the population follows a constant comoving rate density. Assuming that the populations roughly follow the star formation rate, the constant source-frame rate assumption is likely to underestimate the true rate by factors of a few for $1 < z < 3$, and overestimate the rate for $z \gtrsim 3$ (where the true rate density may drop to 0).

To summarize, detectors at Advanced LIGO sensitivity (2G) would find median luminosity distances ($d_{50}^{\rm r}$) for a detected population of 1.4–1.4 $M_\odot$ and 30–30 $M_\odot$ binary coalescences of 202 and 2,440 Mpc, respectively. For 3rd generation detectors this increases to 12 and 30 Gpc. Note that in this latter case the distances are large enough that the evolution of the intrinsic rate density may bias these numbers (generically to higher rate densities at high redshift, and therefore to larger distances). For the recent Advanced LIGO second observing run (O2 sensitivity), the median luminosity distance for a detected population of 1.4–1.4 $M_\odot$ and 30–30 $M_\odot$ binary coalescences is 82 and 942 Mpc, respectively. For the Advanced LIGO third observing run (O3 sensitivity) the corresponding median luminosity distances are expected to be 123 and 1430 Mpc (Abbott et al. 2016b).

For 3rd generation detectors, the Response for 10–10 $M_\odot$ and 30–30 $M_\odot$ binary mergers are far beyond the median and the average distances (see Figure 2). This

indicates that the detector is sensitive to the entire population of sources in the universe, and the detected population is limited by an absence of sources at high redshift. In addition, the comoving volume element turns over and begins to decrease at high redshift, further decreasing the high-redshift sample. Finally, if the source distribution scales with the star formation rate, the population of sources is further reduced at high redshift ($z \gtrsim 2$) as the star formation rate declines.

We note that at low redshift all of the distance quantities are similar ($R \sim d_{50}^{\rm p} \sim d_{50}^{\rm r} \sim d_{50}^{\rm SFR} \sim \bar{d} \sim \bar{d}^{\rm SFR}$ c.f. 1.4–1.4$M_\odot$ binary coalescences in Fig. 1), as would be expected since cosmological effects should become negligible. For configurations with sensitivity at higher redshift these quantities begin to diverge, reflecting interesting cosmological aspects of GW detector sensitivity.

When the "SFR" quantities diverge from their uniform counterparts (e.g., $d_{90}^{\rm SFR}$ compared with $d_{90}^{\rm r}$ in Fig. 2), this is an indication that the evolution of the sources could become an important factor.

4. HOW TO "COSMOLOGIZE" GRAVITATIONAL-WAVE MEASUREMENTS

4.1. Euclid versus Einstein

It has been common within the GW community to use terms such as horizon distance, range, average distance, and sensitive volume. These quantities have generally been defined assuming that space is Euclidean. This is a good approximation so long as we are considering nearby sources, where nearby corresponds to $z \lesssim 0.1$ ($\lesssim 400$ Mpc). Although this applies to NS–NS binaries throughout the advanced LIGO era, for more massive systems we can far exceed this distance. It is therefore advisable to update these quantities so that they properly incorporate cosmology.

In particular, a number of simple scaling relations have come into wide use within the community. For example, Cutler & Flanagan (1994) and Flanagan & Hughes (2005) approximate the BBH waveforms with an inspiral relation, characterizing the SNR with a simple expression: SNR $\propto \mathcal{M}^{5/6}/D$. In addition, the sky sensitivity is described by:

$$\Omega^{1/2}(\theta, \phi, \iota, \psi) = \\ (F_+^2(\theta, \phi, \psi)(1 + \cos^2 \iota)^2 + 4F_\times^2(\theta, \phi, \psi)\cos^2 \iota)^{1/2}, \quad (2)$$

where (θ, ϕ) are the sky locations and (ι, ψ) are the inclination and orientation of the binary. F_+ and F_x are described in Sathyaprakash & Schutz (2009) and Schutz (2011). With ideal sky location and binary inclination and orientation, we find $\Omega = 4$ and the binary can be observed as far as the horizon. For a Euclidean universe, the ratio between the horizon and range distances simplifies to the well know value of 2.26 (Finn & Chernoff 1993). We can therefore estimate the range for BBH sources of chirp mass $\mathcal{M}$ as

$$R = 2\sqrt{\frac{5}{96}} \frac{c(G\mathcal{M}c^3)^{5/6}}{\pi^{-2/3}} \times \frac{2}{2.26} \times \sqrt{I_7}, \quad (3)$$

where the sensitivity of the detector is encapsulated in terms of the moment of the interferometer's noise power

---

[6] TaylorF2 is a frequency-domain, post-Newtonian, inspiral-only, quasi-circular, aligned-spin, binary gravitational waveform approximant.

[7] IMRPhenomD is a frequency-domain phenomenological model gravitational waveform approximant for the inspiral, merger, and ringdown of non-precessing and aligned-spin black-hole binaries.

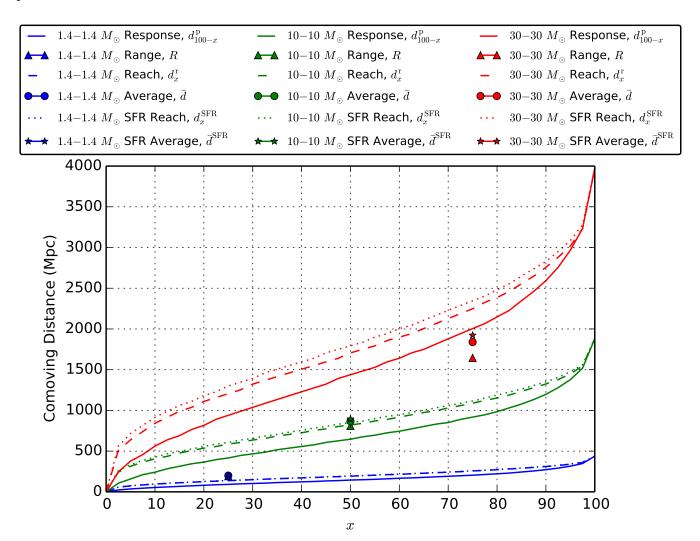|		
—— 1.4−1.4 $M_\odot$ Response, d^{p}_{100-x}	—— 10−10 $M_\odot$ Response, d^{p}_{100-x}	—— 30−30 $M_\odot$ Response, d^{p}_{100-x}
▲▲ 1.4−1.4 $M_\odot$ Range, R	▲▲ 10−10 $M_\odot$ Range, R	▲▲ 30−30 $M_\odot$ Range, R
– – 1.4−1.4 $M_\odot$ Reach, d^{r}_x	– – 10−10 $M_\odot$ Reach, d^{r}_x	– – 30−30 $M_\odot$ Reach, d^{r}_x
●—● 1.4−1.4 $M_\odot$ Average, $\bar{d}$	●—● 10−10 $M_\odot$ Average, $\bar{d}$	●—● 30−30 $M_\odot$ Average, $\bar{d}$
⋯ 1.4−1.4 $M_\odot$ SFR Reach, d^{SFR}_x	⋯ 10−10 $M_\odot$ SFR Reach, d^{SFR}_x	⋯ 30−30 $M_\odot$ SFR Reach, d^{SFR}_x
★—★ 1.4−1.4 $M_\odot$ SFR Average, $\bar{d}^{\mathrm{SFR}}$	★—★ 10−10 $M_\odot$ SFR Average, $\bar{d}^{\mathrm{SFR}}$	★—★ 30−30 $M_\odot$ SFR Average, $\bar{d}^{\mathrm{SFR}}$

FIG. 1.— Distance measures for the design sensitivity of the 2nd generation instrument (2G), corresponding to the fifth sensitivity curve in Figure 1 of Abbott et al. (2016b). The solid line shows the comoving distance at which $(100 - x)$% of the sources would be detected. The dashed line shows the comoving distance within which x% of the total detections would take place, and the dotted line shows the same quantities but scales the source frame rate density by the star formation rate. The triangle, circle, and star are the range, average distance and SFR average distance respectively (see descriptions in Section 2).

spectrum $S_h(f)$:

$$I_7 = \int \frac{f^{-7/3}}{S_h(f)}\, df.$$

However, these simple estimates neglect many important factors: the full inspiral-merger-ringdown waveform, cosmological volume, cosmological redshift, time dilation, and rate density evolution. In what follows we discuss these effects in more detail.

4.2. Antenna pattern

For any set of binary sources at a fixed distance, if you randomly place the sources on the sky at random inclinations and orientations, you get a distribution of measured SNR values. This distribution, when normalized by $\mathrm{SNR_{max}}$, is universal; it is called the *antenna pattern*. It does not depend upon cosmology, the distance, the mass ratio, etc. It also does not depend upon the noise curve, but it does depend on the type of detector (e.g., 2-arm interferometer), number of detectors, the detector orientations, and the relative sensitivities.

This universal single-detector antenna pattern is an incredibly important tool Chernoff & Finn (1993); Schutz (2011). As discussed in more detail in Belczynski et al. (2014, 2015) and especially the appendix of Dominik et al. (2015), we can compress the relevant aspects of the antenna pattern into a single useful function: the cumulative distribution function of the antenna pattern, $P(w)$. Place any CBC source at a *fixed distance*, with a random sky position/inclination/orientation, and measure its SNR in a single GW detector. Let us denote the maximum possible measured SNR as $\rho_{\max}$; this corresponds to a face-on, overhead binary (see discussion below). We ask: what is the probability that this binary might have a measured SNR of ρ or greater (where obviously $\rho \leq \rho_{\max}$)? The answer is given by the cumulative antenna pattern, $P(w)$, with $w = \rho/\rho_{\max}$. A table allowing for simple interpolation of $P(w)$ can be found at `https://github.com/hsinyuc/distancetool`.

Note that if the inclination for all the binaries is fixed (e.g., face-on), and you marginalize over all sky positions, you get a different distribution. This is still universal, in

	$1.4\,M_\odot$–$1.4\,M_\odot$	$10\,M_\odot$–$10\,M_\odot$	$30\,M_\odot$–$30\,M_\odot$
Advanced LIGO 2nd observing run (O2)			
(z, D_L in Mpc, D_C in Mpc)			
Horizon, d^h	(0.04 , 188.9 , 181.3)	(0.19 , 933.8 , 787.0)	(0.46 , 2666.7 , 1821.2)
Redshifted Volume, V_z (Gpc^3)	0.002	0.171	1.95
Range, R (Mpc)	79.8	344.2	775.1
Response, d_{50}^P	(0.01 , 60.1 , 59.3)	(0.06 , 279.8 , 263.8)	(0.15 , 708.4 , 618.6)
Response, d_{10}^P	(0.03 , 115.3 , 112.4)	(0.12 , 551.7 , 494.7)	(0.28 , 1474.8 , 1152.5)
Reach, d_{50}^r	(0.02 , 81.7 , 80.2)	(0.08 , 375.3 , 347.4)	(0.19 , 935.8 , 788.5)
Reach, d_{90}^r	(0.03 , 132.9 , 129.1)	(0.13 , 631.6 , 558.7)	(0.31 , 1680.9 , 1279.8)
SFR Reach, d_{50}^SFR	(0.02 , 82.2 , 80.7)	(0.08 , 382.2 , 353.4)	(0.19 , 974.7 , 816.4)
SFR Reach, d_{90}^SFR	(0.03 , 132.9 , 129.1)	(0.13 , 639.0 , 564.5)	(0.32 , 1724.2 , 1305.9)
Average, $\bar{d}$	(0.02 , 84.2 , 82.6)	(0.08 , 390.7 , 360.7)	(0.2 , 1000.4 , 834.8)
SFR Average, $\bar{d}^\mathrm{SFR}$	(0.02 , 84.5 , 82.9)	(0.08 , 397.1 , 366.1)	(0.2 , 1035.7 , 859.8)
Advanced LIGO 3rd observing run (O3)			
(z, D_L in Mpc, D_C in Mpc)			
Horizon, d^h	(0.06 , 287.5 , 270.6)	(0.29 , 1517.2 , 1179.2)	(0.72 , 4512.8 , 2627.5)
Redshifted Volume, V_z (Gpc^3)	0.007	0.564	5.653
Range, R (Mpc)	118.9	512.7	1105.1
Response, d_{50}^P	(0.02 , 90.6 , 88.8)	(0.09 , 436.3 , 399.4)	(0.22 , 1106.2 , 908.9)
Response, d_{10}^P	(0.04 , 174.5 , 168.1)	(0.18 , 877.6 , 746.0)	(0.42 , 2390.1 , 1679.2)
Reach, d_{50}^r	(0.03 , 122.6 , 119.4)	(0.12 , 578.8 , 516.6)	(0.27 , 1443.2 , 1132.4)
Reach, d_{90}^r	(0.04 , 200.8 , 192.3)	(0.2 , 997.2 , 832.5)	(0.47 , 2693.8 , 1834.8)
SFR Reach, d_{50}^SFR	(0.03 , 123.3 , 120.1)	(0.12 , 597.4 , 531.5)	(0.29 , 1530.1 , 1187.2)
SFR Reach, d_{90}^SFR	(0.04 , 201.5 , 193.0)	(0.2 , 1017.3 , 846.8)	(0.48 , 2792.7 , 1883.7)
Average, $\bar{d}$	(0.03 , 126.8 , 123.4)	(0.13 , 609.9 , 541.5)	(0.29 , 1563.8 , 1208.2)
SFR Average, $\bar{d}^\mathrm{SFR}$	(0.03 , 127.6 , 124.1)	(0.13 , 624.3 , 552.9)	(0.31 , 1638.5 , 1254.1)

TABLE 1

VALUES FOR PROPOSED DISTANCE MEASURES FOR DIFFERENT SOURCE TYPES. O2 AND O3 CORRESPOND TO THE ADVANCED LIGO SECOND AND THIRD SENSITIVITY CURVES IN FIGURE 1 OF ABBOTT ET AL. (2016B).

	$1.4\,M_\odot$–$1.4\,M_\odot$	$10\,M_\odot$–$10\,M_\odot$	$30\,M_\odot$–$30\,M_\odot$
2nd generation (2G)			
(z, D_L in Mpc, D_C in Mpc)			
Horizon, d^h	(0.1 , 482.3 , 437.9)	(0.48 , 2787.9 , 1881.4)	(1.25 , 8931.8 , 3971.0)
Redshifted Volume, V_z (Gpc^3)	0.03	2.22	18.625
Range, R (Mpc)	191.7	809.3	1644.4
Response, d_{50}^P	(0.03 , 149.4 , 144.7)	(0.15 , 750.7 , 651.1)	(0.36 , 1949.8 , 1437.9)
Response, d_{10}^P	(0.06 , 290.0 , 272.9)	(0.29 , 1553.9 , 1202.1)	(0.71 , 4446.9 , 2602.1)
Reach, d_{50}^r	(0.04 , 201.6 , 193.1)	(0.2 , 982.2 , 821.8)	(0.43 , 2420.4 , 1695.1)
Reach, d_{90}^r	(0.07 , 333.2 , 310.9)	(0.33 , 1755.0 , 1324.3)	(0.76 , 4833.3 , 2747.9)
SFR Reach, d_{50}^SFR	(0.04 , 204.0 , 195.3)	(0.2 , 1022.8 , 850.7)	(0.46 , 2610.3 , 1792.8)
SFR Reach, d_{90}^SFR	(0.07 , 335.7 , 313.1)	(0.33 , 1800.3 , 1351.1)	(0.79 , 5053.7 , 2828.0)
Average, $\bar{d}$	(0.05 , 208.9 , 199.8)	(0.21 , 1045.8 , 866.8)	(0.47 , 2701.9 , 1838.8)
SFR Average, $\bar{d}^\mathrm{SFR}$	(0.05 , 210.9 , 201.6)	(0.21 , 1083.4 , 893.1)	(0.49 , 2873.0 , 1922.9)
3rd generation (3G)			
(z, D_L in Gpc, D_C in Gpc)			
Horizon, d^h	(18.57 , 212.5 , 10.9)	(77.2 , 990.7 , 12.7)	(36.4 , 444.1 , 11.9)
Redshifted Volume, V_z (Gpc^3)	315.6	905.7	956.8
Range, R (Gpc)	4.2	6.0	6.1
Response, d_{50}^P	(1.9 , 15.0 , 5.2)	(38.0 , 465.1 , 11.9)	(26.0 , 307.3 , 11.4)
Response, d_{10}^P	(5.9 , 57.9 , 8.4)	(62.4 , 789.7 , 12.5)	(32.3 , 390.3 , 11.7)
Reach, d_{50}^r	(1.6 , 11.9 , 4.6)	(3.3 , 29.0 , 6.8)	(3.4 , 29.9 , 6.9)
Reach, d_{90}^r	(3.9 , 36.1 , 7.3)	(12.9 , 142.1 , 10.2)	(12.0 , 130.9 , 10.0)
SFR Reach, d_{50}^SFR	(1.6 , 11.9 , 4.6)	(2.3 , 19.1 , 5.7)	(2.5 , 20.5 , 5.9)
SFR Reach, d_{90}^SFR	(3.4 , 30.6 , 6.9)	(6.2 , 61.1 , 8.5)	(6.4 , 63.4 , 8.6)
Average, $\bar{d}$	(2.1 , 17.1 , 5.5)	(5.9 , 58.4 , 8.4)	(5.4 , 52.4 , 8.2)
SFR Average, $\bar{d}^\mathrm{SFR}$	(1.9 , 15.4 , 5.2)	(3.3 , 28.7 , 6.7)	(3.3 , 29.6 , 6.8)

TABLE 2

VALUES FOR PROPOSED DISTANCE MEASURES FOR DIFFERENT SOURCE TYPES. 2G CORRESPONDS TO THE ADVANCED LIGO FIFTH SENSITIVITY CURVE IN FIGURE 1 OF ABBOTT ET AL. (2016B), AND 3G CORRESPONDS TO THE "COSMIC EXPLORER (FIG 1)" CURVE OF ABBOTT ET AL. (2017A).
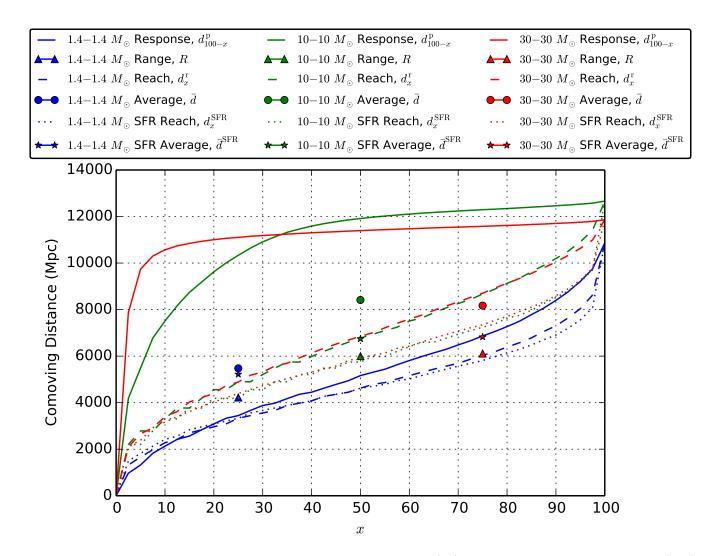
—— 1.4−1.4 $M_\odot$ Response, d_{100-x}^{p}	—— 10−10 $M_\odot$ Response, d_{100-x}^{p}	—— 30−30 $M_\odot$ Response, d_{100-x}^{p}
▲—▲ 1.4−1.4 $M_\odot$ Range, R	▲—▲ 10−10 $M_\odot$ Range, R	▲—▲ 30−30 $M_\odot$ Range, R
— 1.4−1.4 $M_\odot$ Reach, d_x^{r}	— 10−10 $M_\odot$ Reach, d_x^{r}	— 30−30 $M_\odot$ Reach, d_x^{r}
●—● 1.4−1.4 $M_\odot$ Average, $\bar{d}$	●—● 10−10 $M_\odot$ Average, $\bar{d}$	●—● 30−30 $M_\odot$ Average, $\bar{d}$
⋯ 1.4−1.4 $M_\odot$ SFR Reach, d_x^{SFR}	⋯ 10−10 $M_\odot$ SFR Reach, d_x^{SFR}	⋯ 30−30 $M_\odot$ SFR Reach, d_x^{SFR}
★—★ 1.4−1.4 $M_\odot$ SFR Average, $\bar{d}^{\mathrm{SFR}}$	★—★ 10−10 $M_\odot$ SFR Average, $\bar{d}^{\mathrm{SFR}}$	★—★ 30−30 $M_\odot$ SFR Average, $\bar{d}^{\mathrm{SFR}}$

FIG. 2.— Distance measures for one of the proposed 3rd generation instruments (3G), corresponding to the "Cosmic Explorer (fig 1)" curve of Abbott et al. (2017a). The solid line shows the comoving distance at which $(100 - x)\%$ of the sources would be detected. The dashed line shows the comoving distance within which $x\%$ of the total detections would take place, and the dotted line shows the same quantities but scales the source frame rate density by the star formation rate. The triangle, circle, and star are the range, average distance and SFR average distance respectively (see descriptions in Section 2).

the sense that it is independent of cosmology, distance, etc.

Note that if you fix the sky position, but marginalize over all inclinations (e.g., relevant if the antenna pattern of the combined network is spherical), then you get yet a different (still universal) distribution.

In what follows we consider the general case, where the sources are not all at a fixed distance. However, the functional form for $P(> w)$ remains identical, which is a great simplification.

4.3. Euclidean

For $z \lesssim 0.1$, the Universe is well described by Euclidean geometry. In this case we can define the following quantities:

Horizon Distance As discussed briefly in Sec. 1, we consider a single GW detector with a known noise curve. For any given binary coalescence, we define the horizon distance, $d^{\rm h}$ as the maximum distance for which this binary would have an SNR in the detector of at least 8. This corresponds to placing the binary directly overhead (along a line perpendicular to the plane of the detector) and in a face-on configuration (so that the plane of the binary is parallel to the plane of the detector). Any binary detected with SNR $\geq$ 8 must be within this distance. This horizon distance depends on the masses and spins of the source, as well as the noise curve of the detector.

Sensitive Volume Let us assume that we have a uniform rate density of binary coalescence throughout the Universe (e.g., $100 \, {\rm yr}^{-1} \, {\rm Mpc}^3$). The binaries are randomly located and oriented on the sky. We would like to calculate the observable rate of binary coalescence in our detector. Although we can detect binaries as far as $d^{\rm h}$, most binaries will be neither face-on nor overhead, so in practice we are not sensitive to all binaries out to that distance. To calculate the true sensitive volume we need to integrate over the antenna pattern, and average over all binary inclinations and orientations. As discussed in Sec. 4.3, the antenna pattern can be described through a cumulative distribution. This gives the probability that a randomly located/oriented/inclined source *at a given distance* will have a measured SNR $> 8w$, where $0 < w < 1$. The sensitive volume is given by

$$V_{\rm sensitive} = V^{\rm h}/f_p^3, \qquad (4)$$

where $V^{\rm h} = 4\pi (d^{\rm h})^3/3$, and the "peanut factor", f_p, converts between the horizon distance and the sensitive volume. In this expression $d^{\rm h}$ is the comoving distance corresponding to the horizon luminosity distance. We use the term "peanut" because the shape of the sensitive volume is reminiscent of this tasty snack (see for example Schutz (2011)). For Euclidean geometry we have $f_p = 2.264$ Dominik et al. (2015). This factor is independent of the noise curve and the mass of the binary, and is solely a function of the (known) antenna pattern.

4.4. Friedmann-Lemaître-Robertson-Walker

We now generalize these quantities to FLRW cosmologies. Although our approach is general, when we quote numbers or show plots we will assume a standard
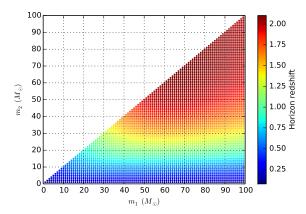

FIG. 3.— Horizon redshift as a function of source frame component masses, assuming 2G sensitivity.

LCDM cosmology with $\Omega_m = 0.3065$, $\Omega_\lambda = 0.6935$, and $h = 0.679$. Percent level changes in these values lead to percent level changes in the distances.

The SNR calculations for a given waveform are identical when generalizing to cosmology, with two important caveats: 1. the distance is now a luminosity distance rather than a Euclidean distance, and 2. the redshifting of the waveform, and therefore the inferred masses, needs to be taken into account (Krolak & Schutz 1987; Holz & Hughes 2005). The sensitive volume definition needs to be generalized to take into account three cosmological effects: 1. the redshifting of the waveform, 2. the redshifting of time, and 3. the cosmological distance and volume factors.

The redshifting of the waveform leads to two general approaches: one can consider a fixed mass in the observer (i.e., LIGO and Virgo) frame, or a fixed mass in the source frame. We now consider each cases in turn.

4.5. Fixed observer frame mass

In this section we assume that a GW detector is measuring a waveform corresponding to a binary with component masses m_1 and m_2, where these are the observer frame masses.

Horizon distance We ask how far a binary with the same *observed* masses could be detected. In this case the calculation is straightforward. The horizon distance is defined exactly as in the Euclidean case, but now the resulting distance is called a luminosity distance. We note that although the observed total mass is M, if the horizon distance for a given binary corresponds to a redshift of $z^{\rm h}$, then the *physical* source frame mass is actually $M/(1 + z^{\rm h})$.

Sensitive volume This calculation is similar to the Euclidean case, except that distance becomes luminosity distance and volume becomes cosmological volume. Along each line-of-sight one can calculate the luminosity distance at which SNR = 8, and we are interested in calculating the volume (in comoving Mpc^3) of this shape.

There are two flavors of sensitive volume, depending on whether one is interested in estimating a number density or a rate density. These sensitive volumes are equivalent if the rate of burst sources is fixed in the *observer* frame. For a rate density fixed in the *source* frame, the rate density sensitive volume is generally less than the
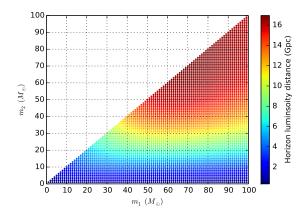
FIG. 4.— Horizon luminosity distance as a function of source frame component masses, assuming 2G sensitivity.

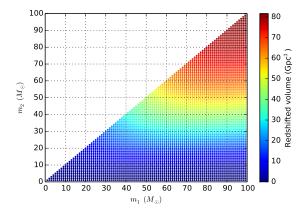

FIG. 5.— Detection-weighted sensitive comoving volume ("redshifted volume") as a function of source frame component masses, assuming 2G sensitivity.

number density sensitive volume because of redshifting in time of the burst sources. For example, if we know that there is 1 (continuous, not burst!) source per comoving Mpc^3, then if we had a number density sensitive volume of $1\,Gpc^3$ we would be able to detect a total of 1×10^9 sources. However, if we assume burst sources with a constant rate in the source frame then the detected rate is impacted by redshifting in time. This is the appropriate case for compact binary coalescence sources, such as the binary mergers detected by LIGO thus far. We then define a detection-weighted sensitive volume, or "redshifted volume" for short, so that multiplying this volume by the source frame rate provides the correct detectable rate:

$$V_{\text{sensitive}} =$$

$$\frac{\int_{D_c < d^{\text{h}}(\theta,\phi,\psi,\iota)} \dfrac{D_c^2}{1 + z(D_c)} dD_c \, d\Omega \sin\iota \, d\iota \, d\psi}{\int \sin\iota \, d\iota \, d\psi}, \quad (5)$$

where $d^{\text{h}}(\theta, \phi, \psi, \iota)$ is the comoving distance for which SNR = 8 for a binary with orientation (ι, ψ) along the sky direction (θ, ϕ). This redshifted volume is less than the number density sensitive volume discussed above, since the redshifting in time always reduces the number of sources detected as one goes to larger distances.

4.6. *Fixed source frame mass*

We now consider the case where the source frame masses are fixed at M, and the observed masses now depend on the redshift of the source: $M_{\text{observed}} = (1+z)M$.

Horizon distance The horizon distance is given by solving for the distance at which a face-on overhead binary will be measured with SNR = 8 for a binary of mass $(1 + z)M$. Values for the horizon redshift as a function of the source frame component masses are shown in Figure 3. The equivalent plot for luminosity distance is shown in Figure 4. The horizon redshift for GW150914 in the Advanced LIGO design sensitivity (2G), keeping the source frame masses fixed, would be 1.33 (corresponding to a horizon luminosity distance of 9,670 Mpc). A web calculator for horizon distance is available at http://gwc.rcc.uchicago.edu.

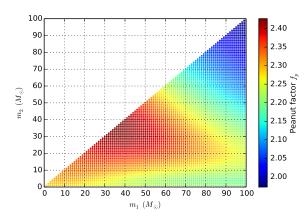**Sensitive volume** The sensitive volume is a similar cal-

FIG. 6.— Peanut factor as a function of source frame component masses, assuming 2G sensitivity.

culation to the fixed observer frame case above. However, since we are now considering fixed source frame masses, we are in effect detecting binaries with different (observer frame) masses at each distance. This distorts the shape of the sensitive volume, and changes the values of peanut factor. In Figure 5 we show the redshifted volume as a function of the source frame masses. The resulting peanut factors are shown in Figure 6. For GW150914, if we fix the mass in the source frame, we find a sensitive volume of $21\,Gpc^3$ and a peanut factor of $f_p = 2.42$.

5. SUMMARY

We have presented a number of quantities to summarize the distance reach of gravitational-wave detectors. In addition to generalizing to luminosity distance and cosmological volumes, and incorporating the antenna pattern sensitivity of the detector, we have also incorporated redshifting of the GW waveform, time dilation of the source rate, and possible evolution of the source frame rate density. We present values for a range of binary systems, and a range of detector sensitivities.

REFERENCES

Abbott, B. P., Abbott, R., Abbott, T. D., et al. 2016a, Physical Review Letters, 116, 131103

—. 2016b, Living Reviews in Relativity, 19, 1

—. 2017a, Classical and Quantum Gravity, 34, 044001

—. 2017b, Physical Review Letters, 118, 221101

Acernese, F., Agathos, M., Agatsuma, K., et al. 2015, Classical and Quantum Gravity, 32, 024001

Allen, B., Anderson, W. G., Brady, P. R., Brown, D. A., & Creighton, J. D. E. 2012, Phys. Rev. D, 85, 122006

Aso, Y., Michimura, Y., Somiya, K., et al. 2013, Phys. Rev. D, 88, 043007

Belczynski, K., Buonanno, A., Cantiello, M., et al. 2014, ApJ, 789, 120

Belczynski, K., Repetto, S., Holz, D., et al. 2015, ArXiv e-prints, arXiv:1510.04615

Chernoff, D. F., & Finn, L. S. 1993, ApJ, 411, L5

Cutler, C., & Flanagan, É. E. 1994, Phys. Rev. D, 49, 2658

Dominik, M., Berti, E., O'Shaughnessy, R., et al. 2015, ApJ, 806, 263

Finn, L. S., & Chernoff, D. F. 1993, Phys. Rev. D, 47, 2198

Flanagan, É. É., & Hughes, S. A. 2005, New Journal of Physics, 7, 204

Hild, S., et al. 2011, Class. Quant. Grav., 28, 094013

Hogg, D. W. 1999, ArXiv Astrophysics e-prints, astro-ph/9905116

Holz, D. E., & Hughes, S. A. 2005, ApJ, 629, 15

Khan, S., Husa, S., Hannam, M., et al. 2016, Phys. Rev. D, 93, 044007

Krolak, A., & Schutz, B. F. 1987, General Relativity and Gravitation, 19, 1163

LIGO Scientific Collaboration, Aasi, J., Abbott, B. P., et al. 2015, Classical and Quantum Gravity, 32, 074001

Madau, P., & Dickinson, M. 2014, ARA&A, 52, 415

Planck Collaboration, Ade, P. A. R., Aghanim, N., et al. 2016, A&A, 594, A13

Sathyaprakash, B., Abernathy, M., Acernese, F., et al. 2012, Classical and Quantum Gravity, 29, 124013

Sathyaprakash, B. S., & Dhurandhar, S. V. 1991, Phys. Rev. D, 44, 3819

Sathyaprakash, B. S., & Schutz, B. F. 2009, Living Reviews in Relativity, 12, 2

Schutz, B. F. 2011, Classical and Quantum Gravity, 28, 125023

Schutz, B. F. 2011, Classical and Quantum Gravity, 28, 125023

Thorne, K. S. 1987, Gravitational radiation., ed. S. W. Hawking & W. Israel, 330–458